CrystEngComm

PAPER

View Article Online
View Journal | View Issue

Cite this: *CrystEngComm*, 2014, **16**, 805

Porous coordination polymers based on azamacrocyclic complex: syntheses, solvent-induced reversible crystal-to-crystal transformation and gas sorption properties†

Xiang Jiang,[a] Zijian Li,[b] Yanyun Zhai,[c] Ge Yan,[a] Hua Xia*[a] and Zhaohao Li*[d]

Received 7th October 2013,
Accepted 30th October 2013

DOI: 10.1039/c3ce42021c

www.rsc.org/crystengcomm

Three microporous coordination polymers, $[NiL]_3[(NiL)(H_2O)_2][(NiL)(TATAB)_2]_2{\cdot}46H_2O$ (**1**), $[(NiL)_3(TATAB)_2]{\cdot}5DMF$ (**2**) and $[(NiL)_3(BTCMT)_2]{\cdot}DMF{\cdot}16H_2O$ (**3**) (L = 1,3,6,9,11,14-hexaazatricyclo[12.2.1.1^{6,9}]octadecane, H_3TATAB = 4,4′,4″-triazine-1,3,5-triyltriaminobenzoic acid and H_3BTCMT = 4,4′,4″-[1,3,5-benzenetriyltris(carbonylimino)]-trisbenzoic acid), were constructed from two tripodal carboxylic ligands and an azamacrocyclic complex. The solvent-mediated, reversible, crystal-to-crystal transformation between **1** and **2** was achieved by immersing the crystalline samples in the corresponding solvent (H_2O or DMF). Furthermore, during the fast bidirectional transformation, solvatochromic behavior was observed and confirmed. The comparison between **2** and **3** indicates that the degree of 6^3 monolayer corrugation has a significant effect on the formation and porous stability of an overall 2D or 3D network. Both **2** and **3** consist of large solvent accessible voids, but only compound **3** possesses permanent porosity, as confirmed by gas adsorption measurements and X-ray powder diffraction. In particular, compound **3** shows a high selective adsorption for CO_2.

Introduction

The rational design and synthesis of microporous materials have attracted considerable attention due to their fascinating structural diversity and functional properties such as gas storage, catalysis, separation, and drug delivery.[1,2] There are several well-known classes of microporous materials, including zeolites, activated carbon, conjugated microporous polymers (CMPs), covalent organic frameworks (COFs), hyper-crosslinked polymers (HCPs), polymers of intrinsic microporosity (PIMs) and microporous coordination polymers (PCPs), *etc.*[2] A honeycomb layered structure is the most ubiquitous structural element in those microporous materials.[3] For example, an overwhelming majority of CMPs/COFs and a large number of HCPs/PCPs are based on honeycomb basic layers (also defined as 6^3 layers from a topological viewpoint).[2,3] Due to their important status in the realm of microporous materials, further thorough and deep explorations of honeycomb layered structures are needed. Among various microporous materials, PCPs are definite crystalline networks constructed from nodes and struts, and their precise structures can be easily determined through single-crystal X-ray diffraction analysis. Therefore, PCPs provide the most straightforward system in the research of honeycomb layers. Typically, to obtain such PCPs based on 6^3 layers, two elementary structural requirements should be met: a 3-connected linker and a 2-connected node. Regarding the former aspect, those tripodal carboxylate groups may serve as ideal linkers. To date, a few tripodal ligands of such geometrical type, namely 1,3,5-benzenetricarboxylate,[4] 4,4′,4″-benzene-1,3,5-triyl-tribenzoic acid,[4] 4,4′,4″-*s*-triazine-2,4,6-triyl-tribenzoic acid,[4] 1,3,5-tris[2-(4-carboxyphenyl)-1-ethynyl] benzene,[5a] and tri(4-carboxy-benzyl)amine[5b] have been utilized for the preparation of PCPs with honeycomb layers. Meanwhile, univalent coinage-metal ions Ag(I)/Cu(I) as 2-connected nodes were often used to generate a wide variety of 6^3 layered-PCP aggregates.[6] Recently, the azamacrocyclic complex had emerged as another smart node choice, because they can provide fixed numbers of vacant coordination sites at axial

[a] *Faculty of Material Science and Chemistry, China University of Geosciences, Wuhan 430074, PR China. E-mail: caihua223@gmail.com*
[b] *School of Chemistry and Chemical Technology, Shanghai Jiao Tong University, Shanghai 200240, PR China*
[c] *College of Chemistry and Chemical Engineering, Xiamen University, Xiamen 361005, PR China*
[d] *College of Chemistry and Chemical Engineering, Luoyang Normal University, Luoyang 471022, PR China. E-mail: lylizh@126.com*

† Electronic supplementary information (ESI) available: Movie 1: immersion of **1** in DMF solution, from yellow to purple. Movie 2: immersion of **2** in H_2O solution, from purple to yellow. X-ray crystallographic file in CIF format, additional figures, gas sorption isotherm and XRD patterns, *etc.* CCDC 963330 (for **1**), 934236 (for **2**) and 913627 (for **3**) contain the crystallographic data for this paper. For ESI and crystallographic data in CIF or other electronic format see DOI: 10.1039/c3ce42021c

positions and enable the extending direction of the network to be controlled.[7]

Crystal-to-crystal transformations (including single-crystal-to-single-crystal) in coordination polymers, which involve cooperative movement of atoms or groups, have emerged as an interesting solid-state phenomenon, which has been utilized to enhance coordination polymers' functionalities, such as gas storage and separation, chemical sensing, catalysis, magnetic switching, and thermal response.[8] Although crystal-to-crystal transformations have been widely observed, the of solid state conversion between azamacrocyclic complex based coordination polymers are still rare.[7j]

In this paper, three new PCPs (Scheme 1), $[NiL]_3[(NiL)(H_2O)_2][(NiL)(TATAB)_2]_2{\cdot}46H_2O$ (**1**), $[(NiL)_3(TATAB)_2]{\cdot}5DMF$ (**2**) and $[(NiL)_3(BTCMT)_2]{\cdot}DMF{\cdot}16H_2O$ (**3**) (L = 1,3,6,9,11,14-hexaazatricyclo[12.2.1.1^{6,9}]octadecane, H_3TATAB = 4,4′,4″-triazine-1,3,5-triyltriaminobenzoic acid and H_3BTCMT = 4,4′,4″-[1,3,5-benzenetriyltris(carbonylimino)]-trisbenzoic acid), were constructed and characterized from two tripodal carboxylic ligands and a hexaaza macrocyclic complex. The crystal-to-crystal transformation between **1** and **2** and the gas sorption properties of **3** are discussed.

Experimental section

The ligands H_3TATAB,[9] H_3BTCMT[10] and $[NiL]{\cdot}(ClO_4)_2$[11] were prepared according to the literature. All the other reagents were purchased commercially and used without further purification. Elemental analyses (carbon, hydrogen and nitrogen) were obtained by a Vario ELIII CHNS/O elemental analyzer. IR spectra were measured from KBr pellets on a Nicolet Avatar 370 Fourier transform infrared spectrometer. Thermogravimetric analyses (TGA) were performed on Diamond TG-DTA 6300 equipment in a flowing N_2 atmosphere with a heating rate of 10 °C min^{-1}. The powder X-ray diffraction measurements were recorded on a Bruker D8 ADVANCE X-ray diffractometer at room temperature. Solid state UV–Vis diffuse reflectance spectra using samples diluted with $BaSO_4$ were recorded with a Shimadzu 2550 PC UV–Vis recording spectrophotometer. Sorption measurements for gases were measured with ASAP-2020M adsorption equipment. Desolvated samples were prepared under a dynamic vacuum (<10^{-3} Torr) at 393 K for 10 h.

Synthesis of 1

In a single tube, an aqueous solution (5 mL) of $[NiL]{\cdot}(ClO_4)_2$ (0.060 g, 0.10 mmol) was layered with a H_2O–CH_3OH (v/v = 1 : 1) solution (5 mL) of Na_3TATAB (0.050 g, 0.10 mmol) at room temperature. After about 2 days, yellow needle-like crystals were obtained between two layers. Yield: 60 mg, 53% (based on $[NiL]{\cdot}(ClO_4)_2$). Anal. calc. for $C_{168}H_{312}N_{60}Ni_6O_{72}$: C, 46.03; H, 7.17; N, 19.17%. Found: C, 45.90; H, 6.89; N, 18.84%. IR data (KBr, cm^{-1}): 3489(s), 3343(m), 3047(s), 2880(m), 1594(m), 1513(m), 1383(s), 1241(w), 1182(w), 1095(m), 1012(m), 836(m), 790(m), 708(m), 502(w).

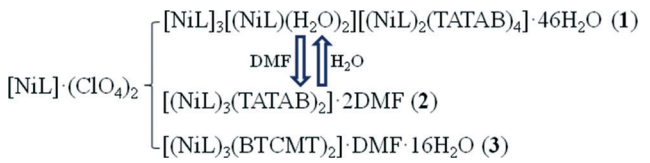

Scheme 1 Synthetic procedures of the title compounds.

Synthesis of 2

In a single tube, a DMF solution (5 mL) of $[NiL]{\cdot}(ClO_4)_2$ (0.060 g, 0.10 mmol) was layered with a H_2O solution (5 mL) of Na_3TATAB (0.050 g, 0.10 mmol) at room temperature. After about two weeks, block purple crystals suitable for X-ray analysis were obtained. Yield: 50 mg, 45% (based on $[NiL]{\cdot}(ClO_4)_2$). Anal. calc. for $C_{99}H_{143}N_{35}Ni_3O_{17}$: C, 52.35; H, 6.05; N, 21.58%. Found: C, 52.89; H, 5.80; N, 21.95%. IR data (KBr, cm^{-1}): 3488(s), 3432(s), 3047(s), 2884(w), 2849(w), 1593(s), 1515(s), 1438(s),1387(s), 1245(m), 1180(w), 1134(w), 1095(m), 1012(m), 986(w), 900(w), 836(m), 791(m), 739(w), 708(m), 503(m).

Synthesis of 3

In a single tube, a DMF solution (5 mL) of $[NiL]{\cdot}(ClO_4)_2$ (0.060 g, 0.10 mmol) was layered with a aqueous solution (5 mL) of Na_3BTCMT (0.057 g, 0.10 mmol) at room temperature. After about 3 days, needle-like purple crystals suitable for X-ray analysis were obtained. Yield: 54 mg, 50% (based on $[NiL]{\cdot}(ClO_4)_2$). Anal. calc. for $C_{99}H_{153}N_{25}Ni_3O_{35}$: C, 48.94; H, 6.35; N, 14.41%. Found: C, 49.20; H, 6.49; N, 14.32%. IR data (KBr, cm^{-1}): 3481(s), 3417(s), 3047(s), 2850(w), 1643(w), 1619(w), 1538(m), 1401(s), 1327(m), 1259(m), 1170(w), 1012(m), 866(w), 835(m), 785(w), 599(w).

Single-crystal X-ray data collection and structure determination

Single crystal X-ray diffraction data for compounds were collected on a Bruker Apex CCD diffractometer with graphite-monochromated Mo-Kα radiation (λ = 0.71073 Å) at 173(2) K. Data reductions and absorption corrections were performed using the SAINT and SADABS programs, respectively.[12] The structures were solved by direct methods using the SHELXS-97 program and refined with full-matrix least squares on F^2 using the SHELXL-97 program.[13] All the non-hydrogen atoms were refined anisotropically. The hydrogen atoms were generated theoretically onto the specific atoms and refined isotropically with fixed thermal factors. The diffraction of this crystal is not good enough. Only extremely small and poorly diffracting crystals were available, and data could be collected with low resolution. Yet the coordination pattern has been established unequivocally. Since there is extensive disorder in the compound **1**, they were located and refined with restraints: similarity restraints (DFIX) have been applied to the geometries of macrocyclic ligands. The anisotropic displacement parameters of some carbon and oxygen atoms have been restrained to have an isotropic behavior (ISOR), due to the instability of their anisotropic refinements. The non-metal atoms and metal atoms (Ni(2) into 0.78 and 0.22; Ni(5) into 0.5 and 0.5)

Table 1 Crystallographic parameters of compounds 1–3[a]

	1	2	3
Chemical formula	$C_{168}H_{312}N_{60}Ni_6O_{72}$	$C_{99}H_{143}N_{35}Ni_3O_{17}$	$C_{99}H_{153}N_{25}Ni_3O_{35}$
Formula weight	4676.82	2271.52	2429.52
Crystal system	Triclinic	Monoclinic	Monoclinic
Space group	$P\bar{1}$	$C2/c$	$P21/c$
a (Å)	8.1401(14)	31.537(5)	8.589(4)
b (Å)	18.984(3)	20.222(5)	17.784(9)
c (Å)	35.484(6)	18.930(4)	38.729(19)
α (°)	97.850(4)	90	90
β (°)	94.141(4)	120.102(4)	102.629(11)
γ (°)	97.048(4)	90	90
Volume (Å^3)	5368.9(15)	10 444(4)	5773(5)
Z	1	4	2
Absorption coefficient (mm^{-1})	0.616	0.620	0.574
Reflections collected	40 554	34 303	20 808
Independent reflections	18 736	9583	10 183
R_{int}	0.073	0.096	0.077
GOF	1.006	1.045	1.013
Final R indices	R_1 = 0.0872	R_1 = 0.0755	R_1 = 0.0693
$[I > 2\sigma(I)]$	wR_2 = 0.2432	wR_2 = 0.1834	wR_2 = 0.1492

[a] GOF = $[\sum w(F_o^2 - F_c^2)^2/(n_{obc} - n_{param})]^{1/2}$; $R_1 = ||F_o| - |F_c||/\sum|F_o|$, w$R_2 = [\sum w(F_o^2 - F_c^2)^2/\sum w(F_o^2)^2]^{1/2}$.

on some macrocycles were modeled to be disordered over two positions of occupancy and SADI restraints for equivalent distances. For the high atomic temperature factor, as compared with bonded neighbors, the anisotropic displacement parameters of some carbon and oxygen atoms have been restrained to be equal (EADP). Because of the disordered solvent molecules in compounds **1–3**, the SQUEEZE routine of PLATON was used to remove the diffraction contribution from these solvents to produce a set of solvent free diffraction intensities.[14] Final formulae were derived from crystallographic data combined with elemental and thermogravimetric analysis data. Details of the crystal parameters, data collection and refinements for the compounds are summarized in Table 1. Selected bond lengths and angles for **1–3** were listed in Tables S1–S3.†

Results and discussion

Compounds **1–3** were insoluble in common organic solvents such as methanol, ethanol, acetonitrile, acetone, dimethylsulfoxide, and DMF. Considering the successful syntheses of those compounds, we hoped to build more interesting PCPs based on 6^3 layers using some analogous tripodal carboxylate ligands instead of H_3TATAB/H_3BTCMT. Although many attempts have been devoted to several analogous ligands, such as 2,4,6-tris-(4-carboxyphenoxy)-1,3,5-triazine, 4,4′,4″-*s*-triazine-2,4,6-triyl-tribenzoic acid, 1,1′,1″-(benzene-1,3,5-triyl)tripiperidine-4-carboxylic acid and 4,4′,4″-(benzene-1,3,5-triyltris(azanediyl))tribenzoic acid (Fig. S1†), it was a pity that no crystals suitable for X-ray diffraction were obtained. Therefore, it should be noted that the deliberate choice of organic ligand plays a crucial role in the self-assembly.

Crystal structures of compounds 1–3

Single-crystal X-ray diffraction analysis reveals that **1** crystallizes in the triclinic space group of $P\bar{1}$. Notably, azamacrocyclic complex segments exist in the structure with three modes (Fig. 1a): (1) dissociative $[NiL]^{2+}$ cation, (2) $[(NiL)(H_2O)_2]^{2+}$ cation with the six-coordinated species that binds two water molecules at the *trans* position on the nickel(II)–azamacrocyclic complex, (3) $[(NiL)(TATAB)_2]^{2-}$ anion in which the nickel(II)–azamacrocyclic complex binds two $[TATAB]^{3-}$ ligands at the axial position. The stoichiometric ratio of $[NiL]^{2+}/[TATAB]^{3-}$ is 3 : 2. Furthermore, those dissociative $[NiL]^{2+}$ cations take part in the solid crystal state through hydrogen-bonding interaction between the $[TATAB]^{3-}$ and the –NH– group on the macrocyclic ligand (Fig. S1†). However, the $[(NiL)(H_2O)_2]^{2+}$ fragment stabilized in the crystal by hydrogen bond formation between the coordinated water molecules and the carboxylate oxygen atoms of $[TATAB]^{3-}$ (Fig. S1†). The packing of compound **1** was mainly directed by intricate bonds, yielding a regular 3D packing network. The water ions are incorporated in the formed channels (Fig. 1b).

The X-ray crystal structure of **2** is shown in Fig. S3.† An asymmetric unit of **2** contains three $[NiL]^{2+}$ cations, two $[BTCMT]^{3-}$ ions and DMF molecules. All of the deprotonated H_3TATAB ligand binds three azamacrocyclic complex fragments in a monodentate mode, and every nickel ion is in a slightly distorted $[NiN_4O_2]$ octahedral coordination geometry, where four nitrogen atoms come from the azamacrocyclic ligand and two oxygen atoms from the carboxylic group oxygen atoms of two $[TATAB]^{3-}$ at the axial positions. When we treat $[TATAB]^{3-}$ as a 3-connected linker and $[NiL]^{2+}$ as a 2-connected node, the framework of **2** can be simplified to a 2D 6^3 network that possesses an undulated arrangement with a thickness of *ca.* 3.7 Å, reflecting a large dihedral angle of 147.3° between adjacent hexagons (Fig. 2a). The large diameter of each honeycomb-like cavity is up to about 37 Å and the 6-membered ring is wave-like, both of which permit the other layers to interpenetrate it in a parallel fashion. In **2**, every single honeycomb-shaped sheet entangles with other

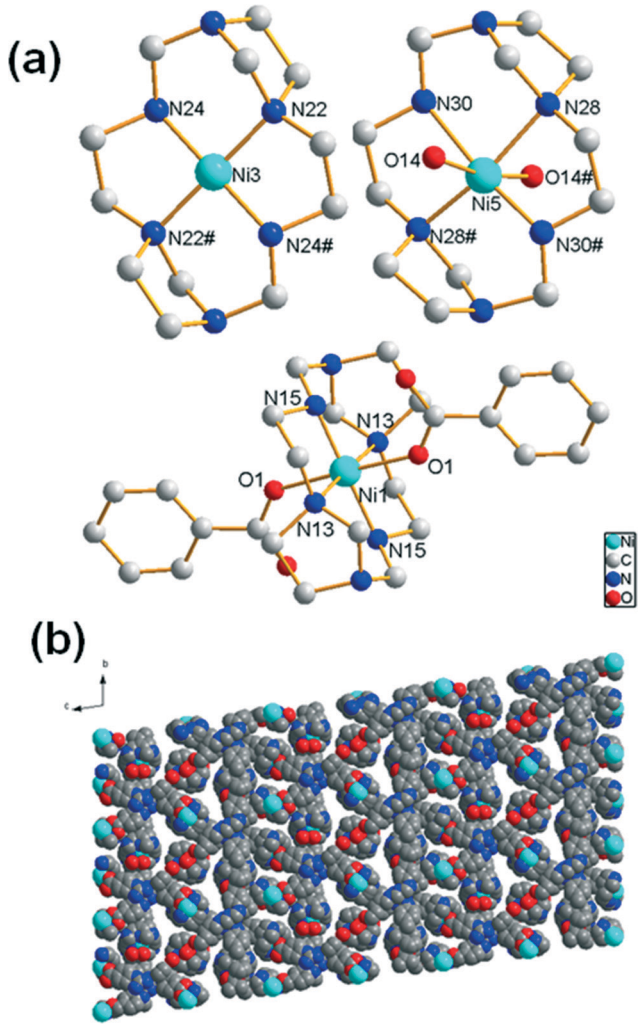

Fig. 1 (a) Three modes of $[NiL]^{2+}$ in compound **1**. #: 2 − *x*, −*y*, −*z*; (b) 1D porous channel in compound **1**.

two equivalent sheets in a repeated interpenetrating fashion, forming a 2D → 2D layer, in which any two of the sheets are not interlocked but the third sheet makes them impartible. This is the typical and unique characteristic of a Borromean structure (Fig. 2b and c). To date, Borromean structures built on azamacrocyclic complexes have rarely been reported.[5,6] 2D Borromean sheets are arranged in ···ABABA··· packing mode (2D → 2D), forming a 1D microporous channel along the *a*-axis (Fig. 2d and e), with the size of 4.2 Å. DMF molecules filled in the channels, and about 20.7% solvent-accessible volume is estimated by using PLATON program.[15]

As shown in Fig. S4,† an asymmetric unit of **3** contains one and a half $[NiL]^{2+}$ cations (a half-occupied $[Ni(1)L]^{2+}$ and a fully-occupied $[Ni(2)L]^{2+}$), and one $[BTCMT]^{3-}$ ion. The coordination environment of Ni(II) in **3** is similar to that in **2**, with all the nickel atoms coordinated to four nitrogen atoms from the azamacrocyclic ligand and two carboxylate oxygen atoms from two $[BTCMT]^{3-}$ ions, showing a slightly distorted $[NiN_4O_2]$ octahedral coordination geometry. The $[BTCMT]^{3-}$ ligand acts as a μ_3-bridge mode, binding three nickel atoms *via* carboxylate groups. As shown in Fig. 3a, we regard $[BTCMT]^{3-}$ as a 3-connected linker and $[NiL]^{2+}$ as a node. Thus, the framework of **2** can be simplified to a 2D infinite honeycomb like the 6^3 basic layer network, which is highly undulated with a thickness of *ca.* 13.7 Å, showing a smaller dihedral angle of 127.1° between adjacent hexagons. The diameter of each honeycomb-like cavity is 24 Å. Such a large cavity allows the honeycomb-shaped sheet to entangle with another two equivalent sheets, forming a 3-fold interpenetrated 2D → 2D sub-layer (Fig. 3b and c). Then, those 3-fold interpenetrated sheets are further entangled with the four adjacent sheets in a parallel fashion, to give an overall unique 2D → 3D dimensional increase network (Fig. 3d). Therefore, the resulting 3D structure can be classified as a "polycatenated network", because the nets have the property that the whole array has a higher dimensionality than that of each component. It can be observed that every 3-fold interpenetrated sheet's nets are involved in entanglement with five adjacent 3-fold layers, summing up to 15 nets. The five entangled adjacent 3-fold layers can also be treated as 5-fold catenation (Fig. 3d). On the other hand, every single 6^3 net is considered to display 7-fold interpenetration (Fig. 3e). As discussed above, the overall 3D network of **2** is formed from intricate entanglement of 6^3 nets by way of both interpenetration and polycatenation. To the best of our knowledge, this type of entanglement had never been reported in those azamacrocyclic complexes based on PCPs. Although the triple interpenetration and 2D → 3D net form to avoid an extremely large void space, **2** still possesses a significant solvent-accessible space (Fig. 3f). Disordered guest molecules are found in the irregular 1D microporous channels with an estimated gate-size of 4.7 × 3.4 $Å^2$ running along the *c*-axis. The void volume in **2** is calculated by PLATON to be 27.0% of the total crystal volume.[15]

Crystal-to-crystal transformation between 1 and 2

Unexpectedly, when the crystalline samples of compound **1** were soaked in DMF, they were completely transformed into compound **2**. The structures of the bulk materials for **1** and **2** were confirmed by PXRD patterns (Fig. S5a–c†). The successful transformation of compound **1** into compound **2** encouraged us to examine its reversibility. When compound **2** was immersed in a H_2O solvent, the PXRD pattern showed that compound **2** was also completely converted to compound **1**, indicating that the transformations between compounds **1** and **2** are reversible under solvent stimuli (Fig. S5d–b†). To our delight, due to the radical changes of nickel(II) coordination environments, solvatochromic behavior was observed during the reversible solvent exchange process (Fig. S6†). To further verify the solvatochromic behavior, the solid state UV–Vis spectra of compounds **1** and **2** were studied (Fig. S7†). The solid state UV–Vis spectrum of compound **1** displays an absorption band with maximum intensity at 450 nm, whereas compound **2** displays an absorption band with maximum intensity at 520 nm, showing an undisputed solvatochromic behavior. Furthermore, as shown in the ESI,†

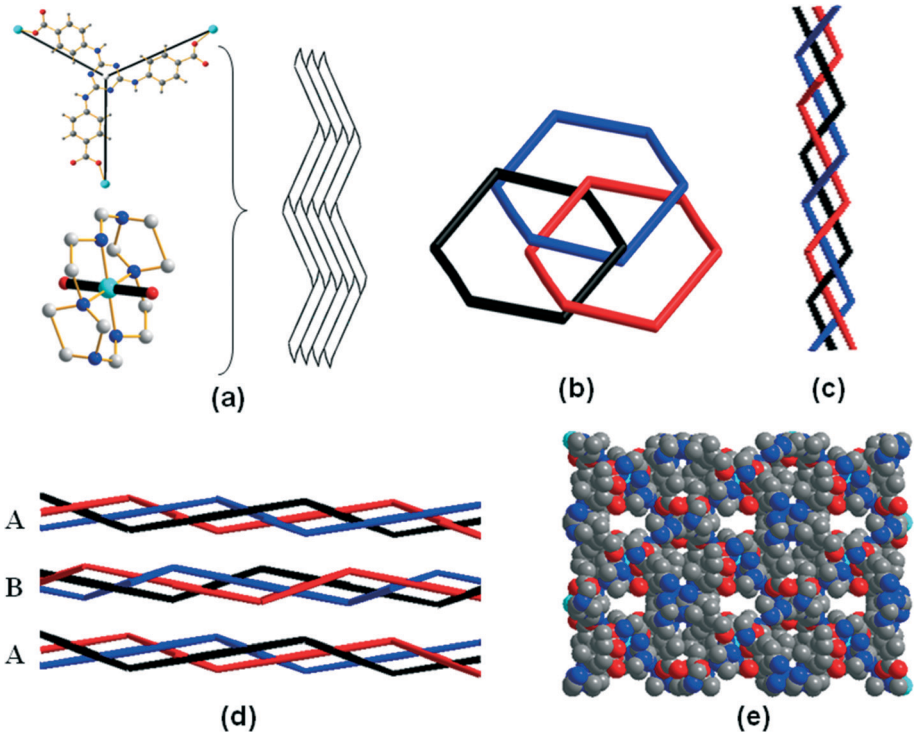

Fig. 2 (a) The topological simplified method and 6^3 layer, (b) the topological structure of the Borromean network, (c) 3-fold interwoven 6^3 sub-layer, (d) 2D → 2D parallel in compound **2**, (e) 1D microporous channel in the *a*-axis direction.

the reversible transformation occurred immediately for the powder. Therefore, as a simple and convenient method, the extremely fast bidirectional transformation in **1** and **2** can be utilized to identify the colorless DMF and H_2O solution.

Structural comparison between compounds 2 and 3

The above structural descriptions of **2** and **3** indicate that the selection of ligands is clearly critical in determining the structures of the resultant compounds. Except for the replacement of the –NH– group with the –CONH– group, H_3TATAB and H_3BTCMT are similar. However, under consistent synthetic conditions, the slight difference between two ligands has a significant influence on the coordination network, and two distinct structures of PCPs have been generated. The results of single crystal X-ray diffraction analyses reveal that both compounds possess a two dimensional (2D) 6^3 network basic layer, and three 6^3 layers interweave in parallel to give rise to either a 2D Borromean layer for **2** or a 3-fold interpenetrating 2D sub-layer for **3**. Furthermore, **2** shows a 2D → 2D → 2D mode, while **3** forms a 2D → 2D → 3D mode. Herein, a comparison of these known 2D → 2D and 2D → 3D examples based on 6^3-hcb layers were presented. Table 2 collects the structural parameters of three parallel interpenetrating 6^3 layers based compounds. As indicated by the summary in Table 2, the synthesis of either the 2D → 2D or 2D → 3D framework from the tripod ligand and linear linker was highly dependent on the thickness of the undulated monolayer or the dihedral angle of adjacent hexagons. For example, due to the fact that the 2D net in **3** is far more corrugated than that in **2**, **3** exhibits a 2D → 3D polycatenation feature rather than the 2D → 2D stacking mode. The final interpenetration number also relies on the degree of 6^3 layers. A lower angle of 6^3 layer (92.4° in ref. 6a) and the most thickness of undulated monolayer (27.0 Å in ref. 6a) lead to the highest degree of 11-fold interpenetration among ever found for 6^3 nets based on coordination bonds.

Since the major difference in the ligands H_3TATAB and H_3BTCMT is –NH– *versus* the –CONH– group, there are some interesting differences in hydrogen bonding interactions between those structures. In **2**, those hydrogen bonding interactions between the secondary amines of L and the uncoordinated carboxylate oxygen atoms of $[TATAB]^{3-}$ are observed ($[d(O–H\cdots N) = 2.894$ Å, $\angle(OHN) = 156.73°]$) (see Fig. S8a†), together with the coordination bond, forming a stable 2D layer. In **3**, those hydrogen bonding interactions between the secondary amines of L and the uncoordinated carboxylate oxygen atoms of $[BTCMT]^{3-}$ are also observed ($[d(O–H\cdots N) = 2.895$ Å, $\angle(OHN) = 155.57°]$). However, different from **2**, the –CONH– groups in H_3BTCMT ligands from adjacent layers form N–H···O hydrogen bonds ($[d(O–H\cdots N) = 2.996$ Å, $\angle(OHN) = 157.50°]$) (Fig. S8b†). Hence, the slightly different hydrogen bond between two ligands may have a significant influence on the overall coordination network.

Stability and sorption properties of compound 2 and 3

Thermogravimetric analyses (TGA) of **1**–**3** indicate that solvent guests were lost in the temperature range 20–100 °C (found 18.91%, calculated 18.49% for **1**), 20–200 °C (found

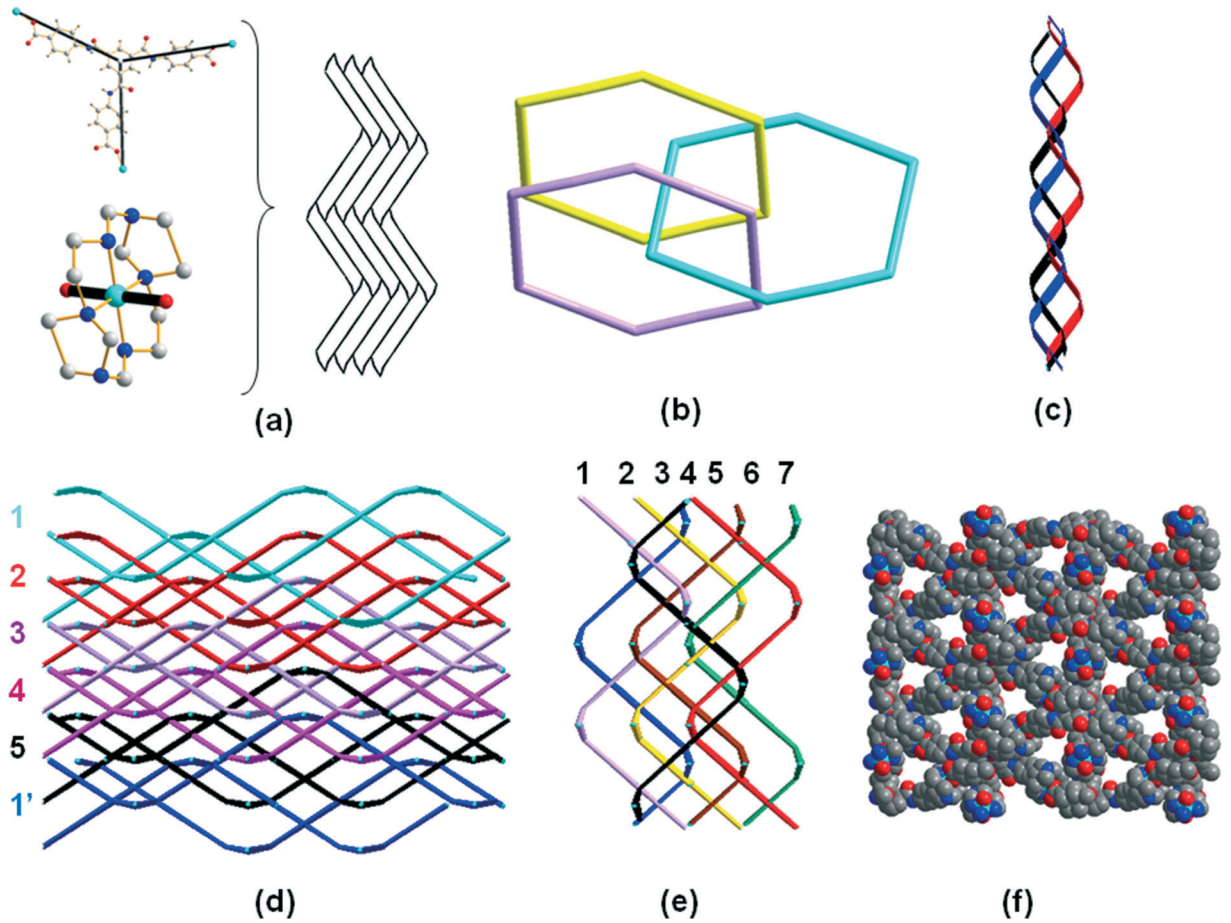

Fig. 3 (a) The topological simplified method and 6^3 layer, (b) the interpenetration unit mode, (c) 3-fold interpenetration sub-layer, (d) simplified representation of the 5-fold catenation, (e) 7-fold interpenetration in compound **3**, (f) 1D microporous channel in the *c*-axis direction.

13.7%, calculated 15.12% for **2**) and 20–260 °C (found 14.68%, calculated 14.86% for **3**), respectively (Fig. S9†). X-ray powder diffraction measurements of both **2** and **3** show that all the peaks displayed in the measured XRD patterns closely match those simulated from the corresponding single-crystal structure, indicating the single phases of **2** and **3** (Fig. S10†). The XRD patterns for desolvated **2** and **3** were recorded under an air atmosphere. The results show that the XRD pattern of **2** changed when the samples were heated, which may be ascribed to the slide between 3-fold interpenetrated layers after the losses of guest molecules (Fig. S10a†). It has been frequently observed in those 2D PCPs that 2D layers slide relative to one another to block the pores when a vacuum is applied to the solid for the gas sorption measurement.[4a,5] The N_2 sorption study on the dried solid of **2** does not exhibit the classically reversible type-I isotherms and gave a Brunauer–

Table 2 The structural parameters of three parallel interpenetrating 6^3 layers based compounds

	Compound	Thickness of undulated monolayer (L Å)	Dihedral angle of adjacent hexagons (θ°)	Stacking mode	Number of interpenetrations	Ref.
Mode 1	$[Ag_2(L_1)_3](BF_4)_2$[a]	3.06	150.7	2D → 2D	3	16
	$[Ag_2(L_2)_3](NO_3)_2{\cdot}7H_2O$[b]	3.40	149.4	2D → 2D	3	17
	$[Ag_2(L_2)_3](NO_3)_2{\cdot}2MeCN$[b]	3.54	148.1	2D → 2D	3	17
	Compound **2**	3.70	147.3	2D → 2D	3	This work
	$[Ni(C_{10}H_{24}N_4)]_3[L_3]_2{\cdot}6C_5H_5N{\cdot}4H_2O$[c]	3.84	146.9	2D → 2D	3	5*a*
	$[(NiL_4)_3(TCBA)_2]$[d]	7.05	141.4	2D → 2D	3	5*b*
Mode 2	Compound **3**	13.7	127.1	2D → 3D	7	This work
	$[Ag_3(tppt)_2](ClO_4)_3{\cdot}8DMSO$[e]	27.0	92.4	2D → 3D	11	6*a*

[a] L_1 = 1,4-bis(2-methylimidazol-1-ylmethyl)benzene. [b] L_2 = 1,1′-methylenebis(3-(pyridin-3-yl)urea). [c] L_3 = 1,3,5-tris[2-(4-carboxyphenyl)-1-ethynyl]benzene. [d] L_4 = 3,10-bis-(2-fluorobenzyl)-1,3,5,8,10,12-hexaazacyclotetradecane, TCBA = tri(4-carboxy-benzyl)amine. [e] tppt = 2,4,6-tris(4-((pyridin-4-ylthio)methyl)phenyl)-1,3,5-triazine.

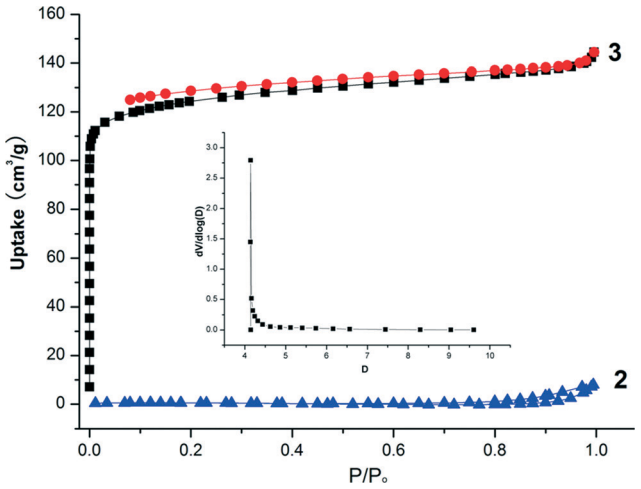

Fig. 4 N_2 sorption isotherms for desolvated **2** and **3** at 77 K; pore size distribution of **3** (inserted figure).

Emmett–Teller (BET) surface area of 1.59 $m^2\ g^{-1}$, indicating the poor porosity of the desolvated solid sample (Fig. 4).

In contrast to **2**, the XRD pattern of the dried solid **3** is consistent with the simulated pattern, indicating that the network structure was unaltered, thus solid **3** possesses permanent porosity (Fig. S10b†). The stability of **3** is due to the enhanced rigidity imposed by the polycatenation interconnecting the 3-fold interpenetrating 2D networks.[18] The N_2 adsorption for desolvated **3** shows a reversible type-I isotherm characteristic of a microporous nature (Fig. 4). The BET and Langmuir surface areas of **3** calculated from the N_2 adsorption isotherm were 421.00 and 554.04 $m^2\ g^{-1}$ respectively, comparable to those reported for PCPs, COFs or porous polymers.[2,3] **3** has a calculated total pore volume of 0.22 $cm^3\ g^{-1}$ based on the N_2 sorption isotherm. The Horvath–Kawazoe mode reveals that the mean pore size of **3** is 4.1 Å, which is in agreement with that calculated from the single crystal structure analysis (Fig. 4 inserted). The CO_2 adsorption isotherm at 195 K for **3** is also type I and the CO_2 uptake capacity at 195 K and 1 atm reaches 185 $cm^3\ g^{-1}$, which is the highest in comparison with other azamacrocyclic ligand based PCPs under the same conditions (Fig. S11†).[6,19]

Once the porosity of **3** is established, we considered their performance in gas storage. In recent years, CO_2 capture or separation is highly attractive for both environmental and economical reasons. PCPs have great potential in CO_2 capture and storage because they can store greater amounts of CO_2 than other classes of porous materials and their chemically-adjustable organic moieties can be carefully pre-designed to be suitable for molecular recognition of CO_2.[1] Hitherto, previous studies indicated that the CO_2 storage and separation

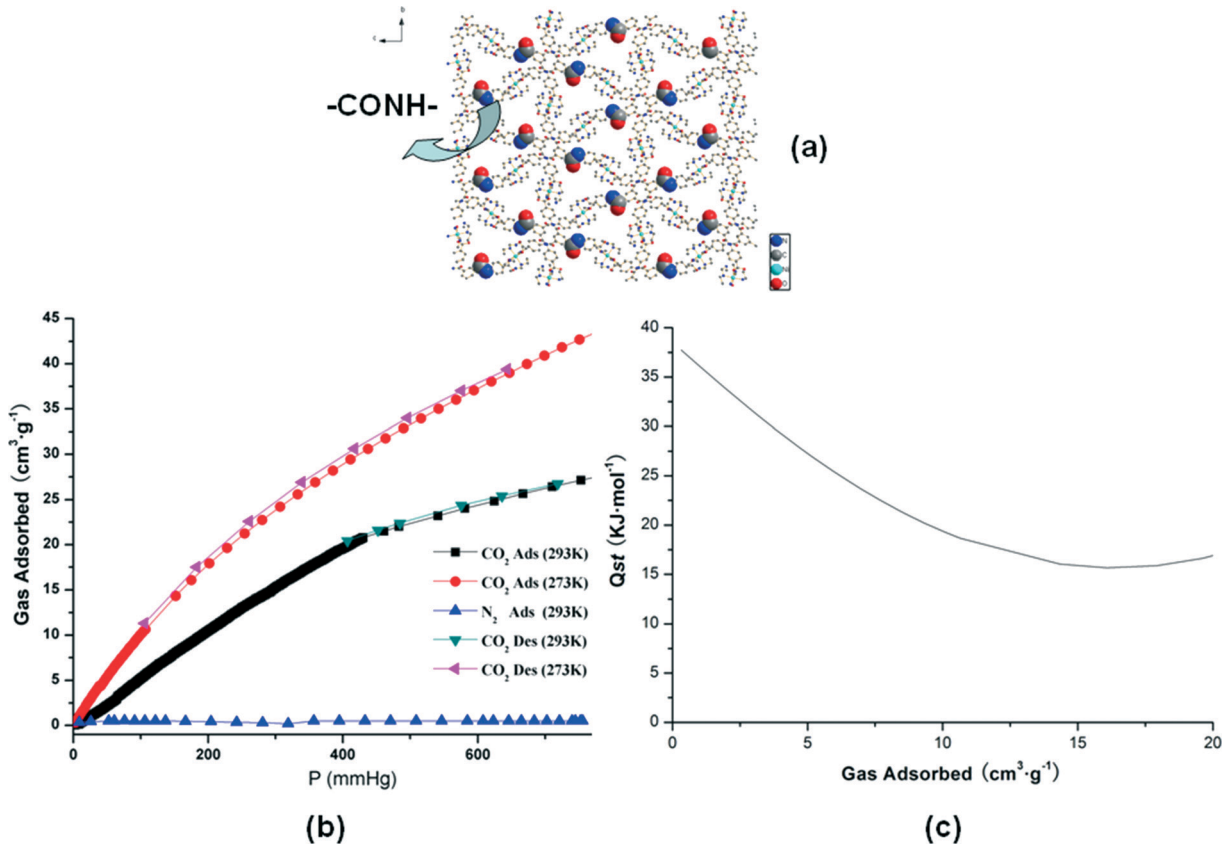

Fig. 5 (a) Acylamide group decorated porous surface, (b) gas sorption curves of N_2 and CO_2 for **3**, (c) isosteric heats of CO_2 adsorption (Q_{st}) values for **3**.

abilities can be dramatically enhanced by generation of specific polar functional groups (–NH_2, –NO_2, –OH, –SO_3^-, –F, *etc.*) within the porous frameworks.[4a,20] Very recently, Bai's groups have successfully inserted –CONH– groups into PCPs, in which those acylamide group decorated PCPs exhibited a strong binding affinity towards CO_2.[20a,21] In compound **3**, part of the acylamide groups are exposed on the channel, resulting in a –CONH– group decorated porous surface (Fig. 5a). To confirm the affinity of **2** towards CO_2 gas, we calculated the isosteric heat of CO_2 adsorption (Q_{st}) for **3** from the sorption isotherms performed at 273 and 293 K according to the Virial 2 model (Fig. S12†). The CO_2 uptakes at 1 atm are 44 $cm^3\ g^{-1}$ (8.7 wt%) at 273 K and 28 $cm^3\ g^{-1}$ (5.5 wt%) at 293 K (Fig. 5b), which are comparable to most PCPs except for PCPs with functionalized groups and coordinatively unsaturated metal centers.[22] Based on the degree of carbon dioxide loading, Q_{st} for CO_2 is within the range of around 15–38 kJ mol^{-1} (Fig. 5c), which is higher than a few reported PCPs materials,[22] but lower than the isosteric heats observed from some functionalised PCP networks, such as MIL-100 (62 kJ mol^{-1}),[23] and ethylenediamine functionalized framework (90 kJ mol^{-1}).[24]

Besides the high CO_2 uptake and reversibility, a high selectivity for CO_2 over N_2 is also one of the necessary properties for a material that can be used as a CO_2 adsorbent. The CO_2/N_2 selectivity of compound **3** was evaluated by the nitrogen adsorption isotherms at 293 K (Fig. 5b). Almost no N_2 adsorption was observed for **3** (0.52 $cm^3\ g^{-1}$ at 293 K and 1 atm). Thus, the result shows the CO_2/N_2 selectivity of **3**. The selective sorption of CO_2 rather than N_2 may be attributed to the large dipole moment of the –CONH– groups, which could facilitate dipole–quadrupole interactions between the acylamide groups in **2** and CO_2, and/or the NH···OCO hydrogen bonds.[20]

Conclusions

In conclusion, with a slight difference of solvent and ligand, three azamacrocyclic complex based microporous PCPs with entirely different structures have been synthesized. Due to the different coordination surrounding environments of the nickel azamacrocyclic complex, extremely fast solvatochromic behavior was observed during reversible crystal-to-crystal transformations between **1** and **2**, and can be used for fast distinction of H_2O/DMF by naked eye recognition of color change within seconds. The comparison of **2** and **3** demonstrates that the different 6^3 layers (thickness of undulated monolayer or dihedral angle of adjacent hexagons) play a crucial role in the formation of their final 2D or 3D architectures, leading to different stability between **2** and **3**. Gas sorption measurements indicate that desolvated **3** can adsorb CO_2 over N_2 molecules, suggesting that **3** has potential for the application of CO_2 separation and storage. In addition, our result provides an effective tactic for the construction of permanently porous PCP through 2D → 3D polycatenation based on honeycomb layer.

Acknowledgements

The work was supported by the Fundamental Research Funds for National University, China University of Geosciences (Wuhan) (no. 1210491B03) and the College Students' Innovative Experiment Project of China (no. 091049148, 111049116). We thank Bo Liu of Northwest University and Kunfu Pi of China University of Sciences (Wuhan) for invaluable suggestions and helping with this work.

References

1 (*a*) G. Ferey, *Chem. Soc. Rev.*, 2008, **37**, 191; (*b*) J. Y. Lee, O. K. Farha, J. Roberts, K. A. Scheidt, S. T. Nguyen and J. T. Hupp, *Chem. Soc. Rev.*, 2009, **38**, 1450; (*c*) J.-R. Li, R. J. Kuppler and H.-C. Zhou, *Chem. Soc. Rev.*, 2009, **38**, 1477; (*d*) L. E. Kreno, K. Leong, O. K. Farha, M. Allendorf, R. P. V. Duyne and J. T. Hupp, *Chem. Rev.*, 2012, **112**, 1105; (*e*) J.-P. Zhang, Y.-B. Zhang, J.-B. Lin and X.-M. Chen, *Chem. Rev.*, 2012, **112**, 1001; (*f*) M. P. Suh, H. J. Park, T. K. Prasad and D. W. Lim, *Chem. Rev.*, 2012, **112**, 782.

2 (*a*) A. Thomas, *Angew. Chem., Int. Ed.*, 2010, **49**, 8328; (*b*) D.-C. Wu, F. Xu, B. Sun, R.-W. Fu, H.-K. He and K. Matyjaszewski, *Chem. Rev.*, 2012, **112**, 3959; (*c*) R. Dawson, A. I. Cooper and D. J. Adams, *Prog. Polym. Sci.*, 2012, **37**, 530; (*d*) R. Dawson, D. J. Adams and A. I. Cooper, *Chem. Sci.*, 2011, **2**, 1173.

3 (*a*) J.-X. Jiang, F. Su, A. Trewin, C. D. Wood, N. L. Campbell, H. Niu, C. Dickinson, A. Y. Ganin, M. J. Rosseinsky, Y. Z. Khimyak and A. I. Cooper, *Angew. Chem., Int. Ed.*, 2007, **46**, 8574; (*b*) A. P. Côté, A. I. Benin, N. W. Ockwig, M. O'Keeffe, A. J. Matzger and O. M. Yaghi, *Science*, 2005, **310**, 1166.

4 (*a*) X.-R. Meng, D.-C. Zhong, L. Jiang, H.-Y. Li and T.-B. Lu, *Cryst. Growth Des.*, 2011, **11**, 2020; (*b*) Y. D. Lampeka, L. V. Tsymbal, A. V. Barna, Y. L. Shuĺga, S. Shova and V. B. Arion, *Dalton Trans.*, 2012, **41**, 4118; (*c*) X.-L. Zhao, H.-Y. He, F.-N. Dai, D.-F. Sun and Y.-X. Ke, *Inorg. Chem.*, 2010, **49**, 8650.

5 (*a*) M. P. Suh, H. J. Choi, S. M. So and B. M. Kim, *Inorg. Chem.*, 2003, **42**, 676; (*b*) L. Jiang, X.-R. Meng, H. Xiang, P. Ju, D.-C. Zhong and T.-B. Lu, *Inorg. Chem.*, 2012, **51**, 1874.

6 (*a*) Q.-Y. Yang, S.-R. Zheng, R. Yang, M. Pan, R. Cao and C.-Y. Su, *CrystEngComm*, 2009, **11**, 680; (*b*) L. Carlucci, G. Ciani and D. M. Proserpio, *Coord. Chem. Rev.*, 2003, **246**, 247.

7 (*a*) Z.-H. Ni, H.-Z. Kou, H.-Y. Zhao, L. Zheng, R.-J. Wang, A.-L. Cui and O. Sato, *Inorg. Chem.*, 2005, **44**, 2050; (*b*) B. Zhang, Z.-H. Ni, A.-L. Cui and H.-Z. Kou, *New J. Chem.*, 2006, **30**, 1327; (*c*) H.-Z. Kou, S. Gao, B.-Q. Ma and D.-Z. Liao, *Chem. Commun.*, 2000, 1309; (*d*) N. Morohashi, F. Narumi, H. Nobuhiko, T. Hattori and S. Miyano, *Chem. Rev.*, 2006, **106**, 5291; (*e*) H. R. Moon and M. P. Suh, *Eur. J. Inorg. Chem.*, 2010, 3795; (*f*) H. J. Choi and M. P. Suh, *J. Am. Chem. Soc.*, 1998, **120**, 10622; (*g*) K. S. Min and M. P. Suh, *Chem.–Eur. J.*, 2001, **7**, 303; (*h*) H. J. Choi, T. S. Lee and M. P. Suh, *Angew. Chem., Int. Ed.*,

1999, **38**, 1405; (*i*) M. P. Suh, J. W. Ko and H. J. Choi, *J. Am. Chem. Soc.*, 2002, **124**, 10976; (*j*) H. J. Choi and M. P. Suh, *J. Am. Chem. Soc.*, 2004, **126**, 15844; (*k*) H. Kim and M. P. Suh, *Inorg. Chem.*, 2005, **44**, 810.

8 (*a*) S. Kitagawa and K. Uemura, *Chem. Soc. Rev.*, 2005, **34**, 109; (*b*) Z.-M. Duan, Y. Zhang, B. Zhang and D.-B. Zhu, *J. Am. Chem. Soc.*, 2009, **131**, 6934; (*c*) B. Moulton and M. J. Zaworotko, *Chem. Rev.*, 2001, **101**, 1629; (*d*) H.-C. Fang, Y.-Y. Ge, H.-Y. Jia, S.-S. Li, F. Sun, L.-G. Zhang and Y.-P. Cai, *CrystEngComm*, 2011, **13**, 67; (*e*) X.-N. Cheng, W.-X. Zhang and X.-M. Chen, *J. Am. Chem. Soc.*, 2007, **129**, 15738; (*f*) Q. Chen, Z. Chang, W.-C. Song, H. Song, H.-B. Song, T.-L. Hu and X. H. Bu, *Angew. Chem., Int. Ed.*, 2013, **52**, 11550; (*g*) J.-R. Li, Y. Tao, Q. Yu, Z.-H. Bu, H. Sakamoto and S. Kitagawa, *Chem.–Eur. J.*, 2008, **14**, 2771; (*h*) S.-M. Zhang, Z. Chang, T.-L. Hu and X.-H. Bu, *Inorg. Chem.*, 2010, **49**, 11581; (*i*) J.-P. Zhao, B.-W. Hu, Q. Yang, T.-L. Hu and X.-H. Bu, *Inorg. Chem.*, 2009, **48**, 7111.

9 (*a*) Q.-R. Fang, D.-Q. Yuan, J. Sculley, J.-R. Li, Z.-B. Han and H.-C. Zhou, *Inorg. Chem.*, 2010, **49**, 11637; (*b*) X.-S. Wang, S. Ma, D. Sun, S. Parkin and H.-C. Zhou, *J. Am. Chem. Soc.*, 2006, **128**, 16474.

10 X. Song, Y. Zou, X. Liu, M. Oh and M. S. Lah, *New J. Chem.*, 2010, **34**, 2396.

11 M. P. Suh, W. Shin, S.-G. Kang, M. S. Lah and T.-M. Chung, *Inorg. Chem.*, 1989, **28**, 1602.

12 *SMART, and SADABS*, Bruker AXS Inc.: Madison, Wisconsin, USA.

13 G. M. Sheldrick, *Acta Crystallogr., Sect. A: Found. Crystallogr.*, 2008, **64**, 112.

14 A. L Spek, *PLATON, A Multipurpose Crystallographic Tool*, Utrecht University, The Netherlands, 2006.

15 A. L. Spek, *J. Appl. Crystallogr.*, 2003, **36**, 7.

16 L. Dobrzanska, H. G. Raubenheimer and L. J. Barbour, *Chem. Commun.*, 2005, 5050.

17 P. Byrne, G. O. Lloyd, N. Clarke and J. W. Steed, *Angew. Chem., Int. Ed.*, 2008, **47**, 5761.

18 (*a*) X.-L. Zhao, J.-M. Dou, D. Sun, P.-P. Cui, D.-F. Sun and Q.-Y. Wu, *Dalton Trans.*, 2012, **41**, 1928; (*b*) H.-L. Jiang, T. A. Makal and H. C. Zhou, *Coord. Chem. Rev.*, 2013, **257**, 2232.

19 H. S. Choi and M. P. Suh, *Angew. Chem., Int. Ed.*, 2009, **48**, 6865.

20 (*a*) B.-S. Zheng, Z. Yang, J.-F. Bai, Y. Li and S. Li, *Chem. Commun.*, 2012, **48**, 7025; (*b*) X.-C. Huang, Y.-Y. Lin, J.-P. Zhang and X.-M. Chen, *Angew. Chem., Int. Ed.*, 2006, **45**, 1557.

21 (*a*) B.-S. Zheng, J.-F. Bai, J. Duan, L. Wojtas and M. J. Zaworotko, *J. Am. Chem. Soc.*, 2010, **133**, 748; (*b*) J. Duan, Z. Yang, J.-F. Bai, B.-S. Zheng, Y. Li and S. Li, *Chem. Commun.*, 2012, **48**, 3058.

22 K. Sumida, D. L. Rogow, J. A. Mason, T. M. McDonald, E. D. Bloch, Z. R. Herm, T.-H. Bae and J. R. Long, *Chem. Rev.*, 2011, **112**, 724.

23 Y. K. Hwang, D. Y. Hong, J. S. Chang, S. H. Jhung, Y. K. Seo, J. H. Kim, A. Vimont, M. Daturi, C. Serre and G. Férey, *Angew. Chem., Int. Ed.*, 2008, **47**, 4144.

24 A. Demessence, D. M. D'Alessandro, M. L. Foo and J. R. Long, *J. Am. Chem. Soc.*, 2009, **131**, 8784.